Calculation of Large-Scale Structure Power Spectra in a Spherical Fourier Bessel Basis

Brandon Khek[1]
Mentors: Olivier Doré[2,3] and Henry Gebhardt[2,3]
[1] *Rice University, Houston, TX, 77005, USA*
[2] *Jet Propulsion Laboratory, Pasadena, CA 91125, USA*
[3] *California Institute of Technology, Pasadena, CA 91109, USA*
(Dated: August 9, 2021)

Upcoming deep (high redshift) wide-angle (large survey area) galaxy redshift surveys such as the High-Latitude Spectroscopic Survey of the Nancy Grace Roman Space Telescope and SPHEREx are estimated to measure the redshifts of millions of galaxies. A spherical Fourier Bessel (SFB) basis for the power spectrum will fully maximize the extraction of cosmological information from this data, and using this basis, we exploit the statistical efficiency of calculations in the Fourier space by naturally separating the angular and radial components over a sphere. In this project, we provide code written in Julia to calculate the SFB power spectrum which is customizable for the parameters set by the survey data and assumed cosmology. By providing robust calculations of the SFB power spectrum, our code will play a crucial role in the analysis of wide-angle galaxy surveys. The code will eventually be leveraged to study how physical effects, such as baryon acoustic oscillations, redshift-space distortions, primordial non-Gaussianity, and modified theories of gravity, manifest themselves in the SFB power spectrum.

I. INTRODUCTION

Cosmology research today strives to characterize the expansion of space, determine the accuracy of general relativity on cosmological scales, and probe the conditions and structures of the early universe. In order to achieve such understanding of the universe, galaxy surveys such as SPHEREx and the Nancy Grace Roman Space Telescope will be launched within the next decade; they will cover large portions of the sky and measure the redshifts of millions of galaxies up to thousands of megaparsecs away. We gain a three dimensional intuition of the universe given by both the radial and angular components of data obtained from these surveys. Because of the large angular separation of observed galaxies, spherical coordinates are the most natural choice for use in analysis.

In this report, we utilize a spherical Fourier Bessel (SFB) basis for our analysis of the matter power spectrum. The basis is named this way due to the fact that we perform calculations in spherical coordinates in Fourier space, and Bessel functions serve as the radial eigenfunction in our basis. The SFB power spectrum can account for wide-angle effects, for we can use a different line of sight for each galaxy observed, unlike in the Cartesian matter power spectrum. In this project we aim to provide accurate and robust code to calculate the SFB power spectrum. We also seek to understand how various physical effects manifest themselves in the power spectrum in anticipation for the data to be received from next-generation galaxy surveys.

In the rest of this section, we will give background information on the power spectrum statistic and physical effects we investigate in this project. In Section II, we derive the SFB power spectrum used in our calculations. Our results are discussed in Section III, separated by which physical effects we are testing, and we estimate the error in our calculations. We conclude in Section IV and end with remarks about further work to be done given the results of this project. Appendix A will discuss the source code developed and used to generate plots in this paper, and appendices B and C elaborate on key optimization techniques used in this code.

A. Physical Effects

1. *Redshift Space Distortions*

It is important to account for Redshift Space Distortions (RSD) in upcoming surveys in order to accurately measure distances to galaxies. RSD occur when light from a galaxy undergoes redshift or blueshift due to the line of sight (LOS) component of the galaxy's peculiar velocity. The inferred distance $\vec{s}(z)$ to a particular galaxy is given by

$$\vec{s}(z) = \vec{r}(z) + \frac{(1+z)\,\vec{v}\cdot\hat{r}}{H(z)}\hat{r}\,, \tag{1}$$

where the first term is the contribution from the Hubble flow, or the expansion of the universe, and the second term is the LOS effect due to the peculiar velocity of the galaxy. The variable z is defined to be the cosmological redshift, $\vec{v}$ is the galaxy's velocity, $\vec{r}$ is the distance to the galaxy we are observing, and $H(z)$ is the Hubble parameter.

The change in wavelength of light due to the velocities introduces bias when measuring the distance to these galaxies solely from their redshifts. However, galaxies moving transversely to the observer's LOS act as a control because of the mitigated effects of extra redshift or blueshift, thus it is still feasible to extract information from these moving galaxy clusters. RSD must be accounted for in the upcoming data so that we can con-

struct an accurate three dimensional map of large scale structure.

2. *Baryon Acoustic Oscillations*

Another key astronomical process to consider are baryon acoustic oscillations (BAO). BAO are useful in measuring distances to cosmological objects because they act as a standard ruler. Before the epoch of recombination, the universe was filled with hot plasma with overdense regions due to quantum fluctuations. Gravity amplified these overdensities, though the coupling of photons and baryonic matter enabled radiation pressure to exert an outward force against the gravitational force, expanding the plasma. The resulting "average" structure of plasma - that is, when taking into account the shape of the many individual overdensities - is a spherical shell with a dark matter center, for dark matter only interacts gravitationally. When the photons decouple from baryonic matter, what is left is a shell of baryonic matter whose known radius - the sound horizon - acts as a cosmological ruler. The imprint of the sound horizon scale shows itself today in galaxy clusters.

The size of the sound horizon helps us distinguish properties of dark energy. Given that we know both the physical and angular size of the sound horizon, we can calculate the distance to the BAO and thus estimate the distance to galaxies. Then, we can measure the redshifts of these galaxies. Repeating this process at many distances allows us to construct the history of cosmic expansion and infer the rate at which the universe expanded. Dark energy, which is responsible for the accelerating rate of the universe's expansion, can then be constrained with this information.

B. Power Spectrum Statistic

The power spectrum is one of the most beneficial statistics used to analyze three dimensional maps of large-scale structure. In the context of our project, we generate the matter power spectrum. The matter power spectrum describes the amount of clustering of matter - galaxies or galaxy clusters in this case - at various length scales. We can expect certain features in the power spectrum, such as BAO or RSD, to shed light on the measurement of cosmological distances. BAO, as mentioned, provide a fiducial scale length, and because the power spectrum is a spectrum of lengths, we can expect subsidiary peaks at the length scale of the BAO.

Furthermore, for RSD, because structures at a higher redshift will be "squished" more along the line of sight due to the Kaiser effect, we can establish a correlation between the amount of distortion to the redshift observed to estimate the distance to the structure. Because the galaxy clusters are more oblate in redshift space, we'd expect the amplitude of the power spectrum to increase compared to if there were no RSD. Observation of RSD at various length scales gives us a sense of what was the typical scale of structures at various distances. Thus, observing RSD and BAO in the power spectrum permits assessment of the growth of structure over time.

II. METHODS

In this section we derive the SFB power spectrum $C_\ell(k,k')$. We begin with the derivation of the continuous SFB power spectrum, that is, with continuous SFB modes. However, boundary conditions imposed by finite survey radii enforces a discretization of the SFB modes, similarly as to how a wave on a string has certain allowable frequencies when fixed at two ends. Thus, we need to account for the survey pixel window, and we discretize the continuous SFB power spectrum in this section as well.

A. Continuous SFB Power Spectrum

Spherical Fourier Bessel modes $\delta_{\ell m}(k)$ are defined by

$$\delta_{\ell m}(k) = \int d^3\vec{r}\left[\sqrt{\frac{2}{\pi}}kj_\ell(kr)Y^*_{\ell m}(\hat{r})\right]\delta(r)\,, \qquad (2)$$

for position $\vec{r} = r\hat{r}$, comoving angular diameter distance r, position on the sky $\hat{r}$, and field $\delta(\vec{r})$ [1]. Considering line-of-sight effects, a radial selection function, and linearly evolving power spectrum, the galaxy density contrast is modeled to linear order as

$$\delta^{\rm obs}(\vec{r}) = \phi(\vec{r})\,D(r)\int\frac{d^3q}{(2\pi)^3}e^{i\vec{q}\cdot\vec{r}}\widetilde{A}_{\rm RSD}(\mu)b(r,q)\delta(\vec{q})\,, \qquad (3)$$

where $\phi(\vec{r})$ is the radial selection function, $D(r)$ is the linear growth factor, $b(r,q)$ is the galaxy bias, $\mu = \hat{q}\cdot\hat{r}$, and $\delta(\vec{q})$ is the matter density contrast in Fourier space. The linear redshift space distortions are

$$\widetilde{A}_{\rm RSD}(\mu) = 1+\beta\mu^2\,, \qquad (4)$$

where we exclude the fingers-of-God effect. Here, $\beta = f/b$, and f is the linear growth rate given by $f = \frac{d\ln D}{d\ln a}$.

We then find the SFB coefficients in the linear universe using Eq. 2 to obtain

$$\delta^{\rm obs}_{\ell m}(k) = \int dq\mathcal{W}_\ell(k,q)\delta_{\ell m}(q) \qquad (5)$$

where the integral kernel $\mathcal{W}_\ell(k,q)$ is given by

$$\mathcal{W}_\ell(k,q) = \frac{2qk}{\pi}\int drr^2\phi(\vec{r})D(r)b(r,q)j_\ell(kr) \times\sum_{\Delta\ell}(\delta^K_{\Delta\ell,0}-\beta f^\ell_{\Delta\ell})j_{\ell+\Delta\ell}(qr) \qquad (6)$$

and the only non-zero $f^{\ell}_{\Delta\ell}$ are

$$f^{\ell}_{-2} = \frac{\ell(\ell-1)}{(2\ell-1)(2\ell+1)} \tag{7}$$

$$f^{\ell}_{0} = -\frac{2\ell^2+2\ell-1}{(2\ell-1)(2\ell+3)} \tag{8}$$

$$f^{\ell}_{2} = \frac{(\ell+1)(\ell+2)}{(2\ell+1)(2\ell+3)}. \tag{9}$$

The SFB power spectrum is then defined as

$$\begin{aligned} C_\ell(k,k') &= \langle \delta^{\rm obs}_{\ell m}(k)\delta^{\rm obs,*}_{\ell m}(k')\rangle \\ &= \int dq\, \mathcal{W}_\ell(k,q)\mathcal{W}^*_\ell(k',q)P(q)\,, \end{aligned} \tag{10}$$

where $P(q)$ is the matter power spectrum in Cartesian coordinates.

B. Discretized SFB Power Spectrum

We consider a survey volume with a maximum radius R, at which we impose a density boundary condition. Application of the boundary condition discretizes the SFB modes. Thus, the following derivation of the discrete SFB power spectrum is motivated by the consideration of finite survey radii. Because the continuous SFB modes $\delta_{\ell m}$ carry more information than the discrete modes, we are only concerned about the transformation from continuous to discrete modes.

The inverse of the continuous Fourier modes and the discrete SFB modes are defined in Eq. (1) and Eq. (44) in [1] by

$$\delta(r) = \int dk \sum_{\ell m} \left[\sqrt{\frac{2}{\pi}} k\, j_\ell(kr) Y_{\ell m}(\theta,\,\phi)\right] \delta_{\ell m}(k)\,, \tag{11}$$

$$\delta_{n\ell m} = \int d^3r\, [g_{n\ell}(r) Y^*_{\ell m}(\hat{r})]\, \delta(r)\,. \tag{12}$$

where $g_{n\ell}$ is given in Eq. (41) in [1]. Though, this is the general form for the superposition of spherical Bessel functions. Because we are only considering a survey with lower bound redshift of zero, the $g_{n\ell}(r)$ take the form

$$g_{n\ell} = c_{n\ell}\, j_\ell(k_{\ell n} r). \tag{13}$$

where the discrete SFB variables are given by

$$k_{\ell n} = \frac{u_{\ell n}}{R} \tag{14}$$

from Eq. (4.2) in [2], for surveys with upper bound radius R. Here, $u_{\ell n}$ is the nth root of a spherical Bessel function of first kind of order ℓ and $c_{n\ell}$ is the normalization factor defined by

$$c_{n_\ell} = \sqrt{2} R^{1.5}\, [j'_\ell(k_{n\ell} R)]^{-1} \tag{15}$$

because we require a density boundary condition at the end of the survey radius [3].

To find a relation between the continuous and discrete SFB modes, we substitute $\delta(r)$ into Eq. 12 and rewrite this as a volume integral with azimuthal angle θ. To get this clearly into the form for the orthogonality relation of spherical harmonics, we move the angular integrals into the sum

$$\begin{aligned} \delta_{n\ell m} = &\int g_{n\ell}(r) \int dk \sum_{L\,M} \sqrt{\frac{2}{\pi}} k\, j_L(kr) \delta_{L\,M}(k) \\ &\times \int_0^{2\pi}\int_0^{\pi} Y^*_{\ell m}(\theta,\phi) Y_{L\,M}(\theta,\,\phi) \sin\phi\, d\phi\, d\theta r^2\, dr. \end{aligned} \tag{16}$$

Application of the orthogonality relation to the equation above yields Kronecker deltas which are only nonzero when $L = \ell$ and $M = m$, thus we can simplify to obtain

$$\delta_{n\ell m} = \int\int c_{n\ell}\, j_\ell(k_{\ell n} r) \sqrt{\frac{2}{\pi}} k\, j_\ell(kr) \delta_{\ell\, m}(k) r^2\, dk\, dr. \tag{17}$$

Multiplying by $\frac{k^2-k^2_{n\ell}}{k^2-k^2_{n\ell}}$ yields a form in which we can use (A3) in Fisher, et al. [3], so we obtain

$$\begin{aligned} \delta_{n\ell m} = -\int \frac{1}{k^2-k^2_{n\ell}} R\, [(k_{n\ell}\, R) j_\ell(kR) j'_\ell(k_{n\ell}\, R)] \times \\ c_{n\ell} \sqrt{\frac{2}{\pi}} k\, \delta_{\ell\, m}(k)\, dk \end{aligned} \tag{18}$$

with a hole at $k = k_{n\ell}$. We can condense this expression to get

$$\delta_{n\ell m} = \int_0^\infty \mathcal{W}^R_{n\ell}(k) \delta_{\ell\, m}(k)\, dk \tag{19}$$

for

$$\mathcal{W}^R_{n\ell}(k) = -\sqrt{\frac{2}{\pi}} \frac{c_{n\ell}\, k}{k^2-k^2_{n\ell}} R\, [(k_{n\ell}\, R) j_\ell(kR) j'_\ell(k_{n\ell}\, R)]\,. \tag{20}$$

Expanding the derivative of the spherical Bessel function using (10.51.2) in [4] and applying the density boundary condition $j_\ell(k_{n\ell}R) = 0$,

$$\mathcal{W}^R_{n\ell}(k) = -\sqrt{\frac{2}{\pi}} \frac{c_{n\ell}\, k\, k_{n\ell} R^2}{k^2-k^2_{n\ell}} j_\ell(kR) j_{\ell-1}(k_{n\ell}R). \tag{21}$$

We can easily find the limit at the hole using L'hopital's rule, so

$$\lim_{k\to k_{n\ell}} \mathcal{W}^R_{n\ell}(k) = -\sqrt{\frac{1}{2\pi}} c_{n\ell}\; k_{n\ell} R^3 j_{\ell-1}(k_{n\ell}R)^2. \tag{22}$$

Therefore, the discretized SFB power spectrum is

$$\begin{aligned} \langle \delta_{n\ell m}\, \delta_{n'\ell' m'}\rangle = \delta^K_{\ell,\ell'} \delta^K_{m,m'} \times \\ \int_0^\infty \int_0^\infty \mathcal{W}^R_{n\ell}(k) \mathcal{W}^R_{n'\ell'}(k') C_\ell(k,k')\, dk\, dk'. \end{aligned} \tag{23}$$

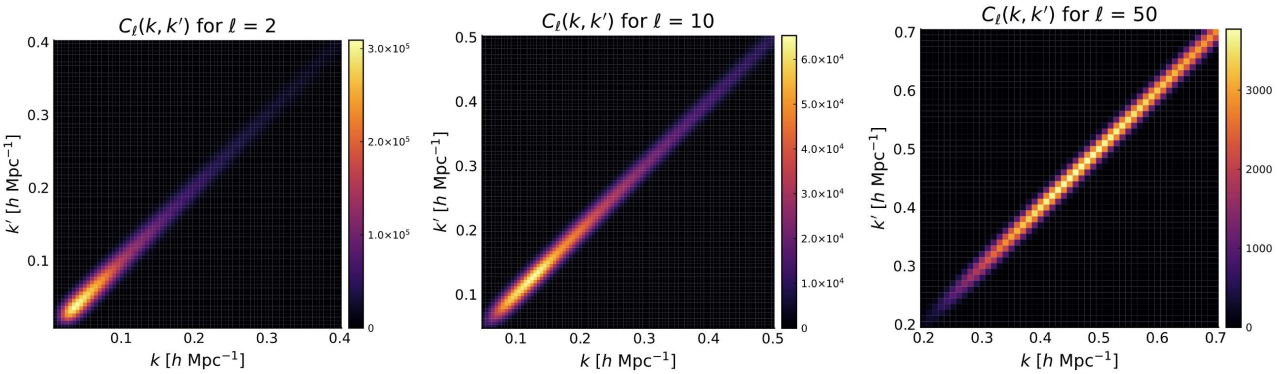

FIG. 1: SFB power spectrum $C_\ell(k,k')$ for various ℓ.

III. RESULTS

Unless otherwise noted, the results presented will display the continuous SFB power spectrum for redshift dependent bias $b(z) = \sqrt{1+z}$ and radial selection function $\phi(r) = e^{-r^2/r_0^2}$ for $r_0 = 150\,h^{-1}$ Mpc. We ignore the fingers-of-God effect and investigate each physical effect independently of one another. For our cosmology, we assume the Planck cosmological parameters in a flat ΛCDM universe.

The most basic form of the SFB power spectrum, with only the growth of structure and BAO but no RSD or non-Gaussianity, is displayed in Figure 1. As we go to higher ℓ modes, the peak of the power spectrum shifts to larger k, or smaller length scales. This can be explained by the fact that larger ℓ modes correspond to smaller divisions across the sphere, thus the clustering amplitude peaks at these smaller scales.

1. *BAO and RSD*

While a 2D heatmap of $C_\ell(k,k')$ gives a sense of the shape of the SFB power spectrum across a large range of k, BAO are easier to resolve with a higher resolution in our plot, as displayed in Fig. 2. Notice how the power spectrum has bumps around 10^{-1} h Mpc^{-1}. The bumps tell us the length scale of the sound horizon which demonstrates how BAO serve as a cosmological ruler.

We can extend the BAO plot by also including RSD. The clustering amplitude increases, as shown in Fig. 3. This expected result arises from the fact that the infall of galaxies along the LOS results in additional redshift or blueshift if they are moving away or toward us. This redshift alters our inferred distance to the galaxies, resulting in the perception that they are further if they undergo additional redshift, or closer if they undergo additional blueshift. Otherwise circular structures would appear oblate, and this would in turn increase the amount of clustering we measure.

A two dimensional view of the power spectrum also shows an increase in the maximum clustering amplitude,

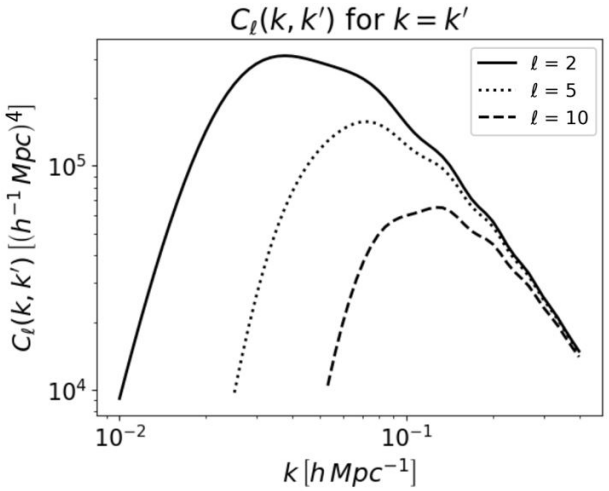

FIG. 2: BAO are best seen in the SFB power spectrum along the diagonal $k = k'$.

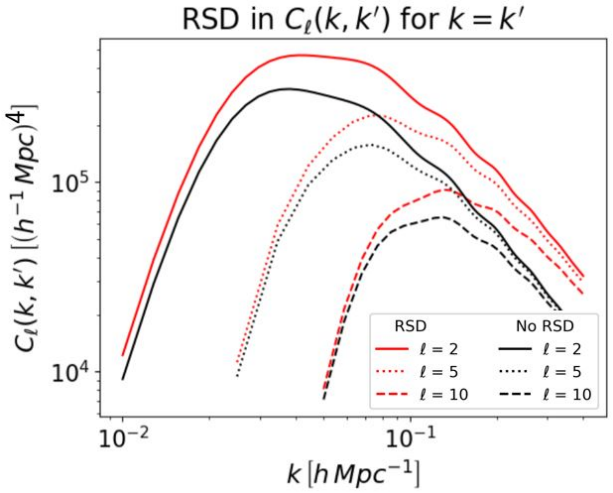

FIG. 3: The SFB power spectrum with redshift space distortions are displayed in red and without RSD in black. The solid line represents the power spectrum with the $\ell = 2$ mode, the dotted line corresponds to $\ell = 5$, and the dashed line is for $\ell = 10$.

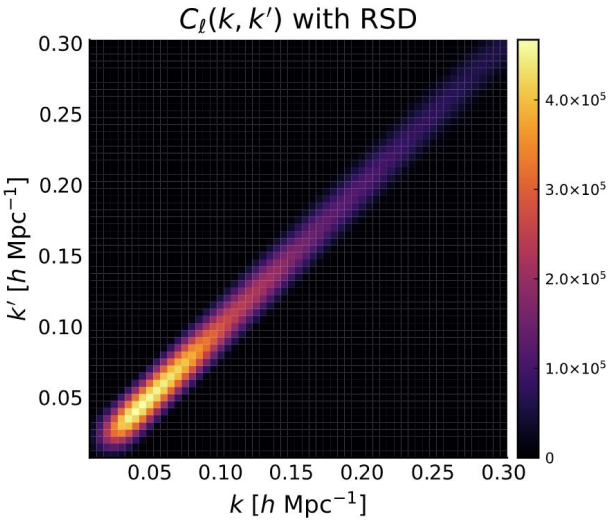

FIG. 4: The SFB power spectrum for $\ell = 2$ with redshift space distortions. We see approximately a $1.3 * 10^5$ increase in the maximum amplitude compared to $C_\ell(k, k')$ with no RSD.

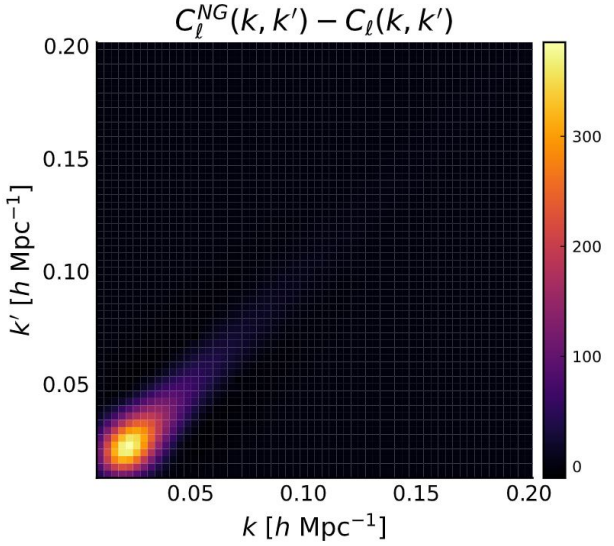

FIG. 5: The SFB power spectrum $C_\ell^{NG}(k, k')$ computed with the bias function corrected for non-Gaussianity subtracted by the SFB power spectrum with the usual redshift dependent bias $b = \sqrt{1+z}$. The maxima of $C_\ell^{NG}(k, k')$ and $C_\ell(k, k')$ are $310,129$ and $309,992$ $(h^{-1}\text{Mpc})^3$, respectively.

as shown in Fig. 4. The width of the diagonal may change, and the extent at which RSD affects the power spectrum is to be studied in the future.

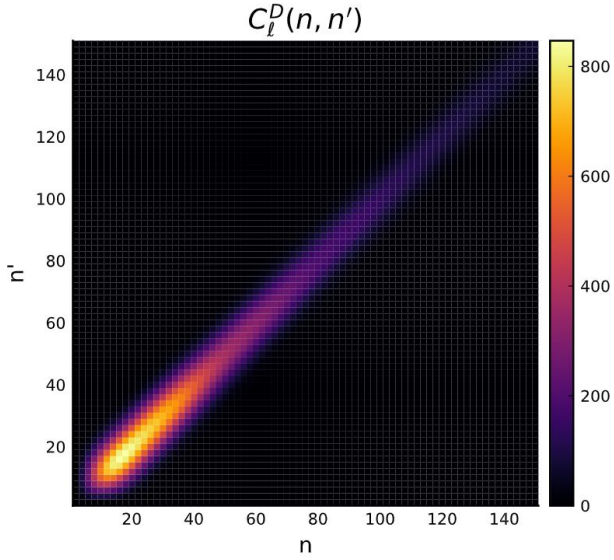

FIG. 6: SFB power spectrum $C_\ell^D(n, n')$ with discretized modes considered with a survey of radius 1500 h^{-1} Mpc. The approximate range of k that the n correspond to is 0.01 to 0.3 h Mpc^{-1}.

2. *Non-Gaussianity*

We now investigate the effects of non-Gaussianity on the SFB power spectrum. Studying non-Gaussian effects requires the use of a scale and redshift dependent bias. A corrective term is added to our usual redshift dependent bias $b(z) = \sqrt{1+z}$ to account for non-Gaussianity, so our adjusted galaxy bias is

$$b(z,k) = b(z) + 2(b(z)-1) f_{NL} \delta_c \frac{3\Omega_m}{2a\, D(a) r_H^2 k^2} \qquad (24)$$

where δ_c is the critical overdensity, $D(a)$ is the linear growth factor, and f_{NL} describes the higher order dependence of the amplitude of non-Gaussian effects. In previous experiments such as eBOSS, we have found the constraint that $|f_{NL}| \lesssim 10$, and here we take it to be 100 for the purposes of illustrating the difference in the power spectrum with and without this effect [5]. The resulting plot is shown in Fig. 5. The majority of the difference arises at $k < 0.05\, h$ Mpc^{-1}. That is, non-Gaussian effects are only noticeable on large scales.

3. *Discrete SFB Power Spectrum*

The discrete SFB power spectrum $C_\ell^D(n, n')$ is more in line with what we expect to measure from upcoming survey data due to their finite radius. Instead of measuring the power spectrum as a gamut of continuous length scales, we instead measure it at discrete modes $k_{n\ell}$.

It must be noted that in the plot shown in Fig. 6, the SFB power spectrum we generated has a much smaller

TABLE I: Estimated Error and Computation Time for $C_\ell(k, k')$

ℓ	**k Range (h/Mpc)**	**Average % Error**	**Time (s)**
2	0.01 to 0.3	1.7×10^{-11}	1.71
10	0.05 to 0.4	1.1×10^{-4}	1.27
50	0.15 to 0.5	1.2×10^{-2}	5.37

amplitude compared to the continuous power spectrum. The discrepancy most likely arises due to the fact that transformation performed in Eq. 12 changed the units we measure the discrete SFB power spectrum in from those used in the continuous SFB power spectrum. Nonetheless, the shape of the power spectrum is maintained as expected, for the discretization of the modes should only affect the scale at which the spectrum is generated, and in this case it is dependent on discrete n.

4. Estimated Error and Runtime

Error can arise due to the precision of our numerical integration technique. We use Gauss-Legendre Quadrature for our calculations, so the error would largely stem from the number of nodes we use (for more information, see Appendix B). We calculate the error for the $C_\ell(k, k')$ calculation by computing $C_\ell(k, k')$ along $k = k'$ for various ℓ modes. The range of k that we use will vary because we focus on the region near where the power spectrum peaks. However, because higher ℓ shift the peak toward larger k, the argument to the spherical Bessel functions defined in Eq. 6 increases, resulting in a larger frequency. Hence, higher precision, or more nodes, is required at larger ℓ to maintain accuracy. For all of the ℓ modes, we use 750 nodes and compare our results to $C_\ell(k, k')$ computed with 1500 nodes. The results are displayed in Table I.

The number of nodes used is the major factor that contributes to the calculation times. Clearly, we can use less nodes for low ℓ modes. For example, for $\ell = 2$ with 500 nodes, computation time is 0.74 seconds and we achieve 0.005% error.

IV. CONCLUSIONS AND FUTURE WORK

In this project, we created accurate and efficient code that calculates the SFB power spectrum, adjustable to account for physical effects like RSD and non-Gaussianity. Notable ways in which these effects appeared in the power spectrum were an increase in the clustering amplitude at large scales and increase in amplitude along the diagonal $k = k'$ for non-Gaussianity and RSD, respectively. Our code enables us to study how these effects appear in the power spectrum which ultimately prepares us to analyze data in next-generation galaxy surveys.

With the foundation of the code module set, there are many avenues to continue our studies. Namely, we look forward to studying the effects of theories of modified gravity in the power spectrum, investigating the behavior of the off-diagonal terms further, improving the speed of our code, and of course applying our code to real data.

ACKNOWLEDGMENTS

I'd like to give immense thanks to Henry Gebhardt for his kind guidance and significant insights at every one of our meetings. I am very grateful for the time he devoted to not only the project, but also to ensuring that I am well versed in scientific communication and strongly grounded in fundamental cosmology knowledge. I'd also like to give many thanks to Olivier Doré for creating an incredibly welcoming environment and for his encouragements to reach out to others. Finally, I'd like to thank the JPL "Dark Sector" for their dedication to the SURF students, namely Peter Taylor for organizing and leading our weekly meetings, as well as Chen Heinrich, Agnes Ferte, Kris Pardo, and Lluis Mas-Ribas for their mini-lectures on skills and advice useful for a career in astrophysics and cosmology. I find it spectacular to have been able to learn so much from all of them.

Appendix A: Julia Package

The Julia package we developed and used for this paper will soon be publically available on GitHub, pending approval by JPL. In it, we also include an ancillary design document that outlines the entire module as well as the corresponding theory used.

Appendix B: Gauss-Legendre Quadrature

The Gauss-Legendre quadrature integration algorithm is crucial in our optimization of our code. The integral approximation takes the form of

$$\int_{-1}^{1} f(x)dx \approx \sum_{i=1}^{n} w_i f(x_i) \tag{B1}$$

for nodes x_i and weights w_i. We utilize the Julia module `FastGaussQuadrature.jl` [6] to implement this algorithm. In our program, it is used to compute the integral kernel $W_\ell(k, q)$. Because the kernel is defined as an integral from 0 to ∞, we want to find a function $t : [0, \infty) \to [-1, 1]$ to get our integrand into the form of Eq. B1. We choose $t(r) = 2\tanh(10^{-4}r) - 1$. We chose the 10^{-4} factor for r because it helps "spread out" the interval such that we don't reach the $y = 1$ asymptote too quickly, thus we require less computational precision

for large r. Solving for r, we obtain

$$r(t) = 10^4 \text{arctanh}\left(\frac{t+1}{2}\right) \tag{B2}$$

$$dr = \frac{5000}{1-0.25(t+1)^2} \tag{B3}$$

to substitute into Eq. (6).

Appendix C: Width Estimate of $\mathbf{W}_\ell(\mathbf{k},\mathbf{q})$

Because the SFB power spectrum $C_\ell(k,k')$ is defined by an integral over the kernels $W_\ell(k,k')$ as given in Eq. 11, we need to find the bounds of integration that allow us to approximate the integral without having to evaluate it over the entire positive real line. We can exploit the fact that the kernels are very sharply peaked and almost zero outside of the width of this peak. Therefore, in this section we derive a width estimate - akin to an equivalent width - of these kernels, and this analytic approximation for the width is pivotal in making our calculation of the SFB power spectrum efficient.

Limber's approximation [7] can be distilled down to a substitution

$$j_\ell(kr) \approx \sqrt{\frac{\pi}{2kr}}\delta^D\left(kr-\ell-\frac{1}{2}\right). \tag{C1}$$

We make the above approximation in Eq. 6, obtaining

$$\mathcal{W}_\ell(k,q) = \sqrt{kq}\int dr\, r\, \phi(r)\, D(r)\, b(r,q)\delta^D(kr-\ell-\frac{1}{2}) \times \sum_{\Delta\ell}(\delta^K_{\Delta\ell,0}-\beta f^\ell_{\Delta\ell})\delta^D(qr-\ell-\Delta\ell-\frac{1}{2}) \tag{C2}$$

which is only nonzero for $r = \frac{\ell+1/2}{k}$. Substituting for r, multiplying by $\sqrt{k}/\sqrt{k}$, and factoring $\frac{\ell+1/2}{k}$ from the delta function inside the sum yields

$$\mathcal{W}_\ell(k,q) = \sqrt{\frac{q}{k}}\,\phi\left(\frac{\ell+\frac{1}{2}}{k}\right) D\left(\frac{\ell+\frac{1}{2}}{k}\right) b\left(\frac{\ell+\frac{1}{2}}{k},q\right) \times \sum_{\Delta\ell}(\delta^K_{\Delta\ell,0}-\beta f^\ell_{\Delta\ell})\delta^D\left(q-\frac{\ell+\Delta\ell+\frac{1}{2}}{\ell+\frac{1}{2}}k\right) \tag{C3}$$

For $\Delta\ell \ll \ell$, we require $k \approx q$, so the delta function in the sum effectively becomes $\delta^D(q-k)$. Integration over the kernel is only nonzero for $k=q$, thus

$$\int_0^\infty W_\ell(k,q)\,dq \approx \phi\left(\frac{\ell+\frac{1}{2}}{k}\right) D\left(\frac{\ell+\frac{1}{2}}{k}\right) b\left(\frac{\ell+\frac{1}{2}}{k},q\right) \times \sum_{\Delta\ell}(\delta^K_{\Delta\ell,0}-\beta f^\ell_{\Delta\ell}) \tag{C4}$$

and the width estimate, which we term the *equivalent width* w of the kernel, is given by

$$w = \frac{\int_0^\infty W_\ell(k,q)\,dq}{W_\ell(k,k)} \tag{C5}$$

with the assumption that the maximum of $W_\ell(k,q)$ occurs when $k=q$.

To calculate our integration bounds for $C_\ell(k,k')$ in this project, we first find two intervals for each $W_\ell(k,q)$ in Eq. 11. The intervals are defined by being the size of two equivalent widths centered at $k=q$. Then, we only integrate over the region in which the intervals for both integral kernels overlap. That is, we assume the integrand is 0 outside of this interval.

[1] H. Gebhardt and O. Doré, Superfab: a fabulous code for spherical fourier-bessel decomposition (2021).

[2] M. Wang, S. Avila, D. Bianchi, R. Crittenden, and W. Percival, Hybrid-basis inference for large-scale galaxy clustering: combining spherical and cartesian fourier analyses, Journal of Cosmology and Astroparticle Physics **2020** (10), 022.

[3] K. B. Fisher, O. Lahav, Y. Hoffman, D. Lynden-Bell, and S. Zaroubi, Wiener reconstruction of density, velocity, and potential fields from all sky galaxy redshift surveys, Mon. Not. Roy. Astron. Soc. **272**, 885 (1995).

[4] Bessel functions; spherical bessel functions; recurrence relations and derivatives, https://dlmf.nist.gov/10.51#E2, accessed: 2021-08-06.

[5] N. Dalal, O. Doré, D. Huterer, and A. Shirokov, Imprints of primordial non-gaussianities on large-scale structure: Scale-dependent bias and abundance of virialized objects, Phys. Rev. D **77**, 123514 (2008).

[6] https://github.com/JuliaApproximation/FastGaussQuadrature.jl.

[7] D. N. Limber, The Analysis of Counts of the Extragalactic Nebulae in Terms of a Fluctuating Density Field. II., Astrophys. J. **119**, 655 (1954).